
Neural Optimal Control for Representation Learning

Mathieu Chalvidal^{1,2,3}, Matthew Ricci², Rufin VanRullen^{1,3}, Thomas Serre^{1,2}

¹Artificial and Natural Intelligence Toulouse Institute, Université de Toulouse, France

²Carney Institute for Brain Science, Dpt. of Cognitive Linguistic & Psychological Sciences
Brown University, Providence, RI 02912

³Centre de Recherche Cerveau & Cognition CNRS, Université de Toulouse
UMR 5549, Toulouse 31055 France

{mathieu_chalvid, matthew_ricci_1, thomas_serre}@brown.edu
rufin.vanrullen@cnrs.fr

Abstract

The intriguing connections recently established between neural networks and dynamical systems have invited deep learning researchers to tap into the well-explored principles of differential calculus. Notably, the adjoint sensitivity method used in neural ordinary differential equations (Neural ODEs) has cast the training of neural networks as a control problem in which neural modules operate as continuous-time homeomorphic transformations of features. Typically, these methods optimize a single set of parameters governing the dynamical system for the whole data set, forcing the network to learn complex transformations that are functionally limited and computationally heavy. Instead, we propose learning a data-conditioned distribution of *optimal controls* over the network dynamics, emulating a form of input-dependent fast neural plasticity. We describe a general method for training such models as well as convergence proofs assuming mild hypotheses about the ODEs and show empirically that this method leads to simpler dynamics and reduces the computational cost of Neural ODEs. We evaluate this approach for unsupervised image representation learning; our new “functional” auto-encoding model with ODEs, AutoencODE, achieves state-of-the-art image reconstruction quality on CIFAR-10, and exhibits substantial improvements in unsupervised classification over existing auto-encoding models.

1 Introduction

Ordinary differential equations (ODEs) have been used to express the laws of most theories of physics and have found applications in scientific disciplines as diverse as computer vision, epidemiology, economy, genetics, neuroscience, and climatology to name a few. A popular framework for modeling neural activity in both neuroscience and deep learning is that of dynamical systems [1–4]. For instance, the analysis of neural responses in the motor cortex has revealed complex temporal dynamics shown to be well modeled by artificial recurrent neural models [5].

In parallel, so-called Neural ODEs [6] have cast neural network computations as continuous-time *orbits* of dynamical systems that can be approximated on the fly by an ODE solver, leveraging the adjoint sensitivity method of [7] to efficiently learn a parametrization of the dynamics. However, similar to the standard deep learning setting, this approach optimizes a static set parameters defining one dynamics for the whole data distribution. After training, a single dynamical system must account for each model input. Compare this to biological neural processing, where different tasks give rise to a multitude of dynamical regimes and attendant computations [8].

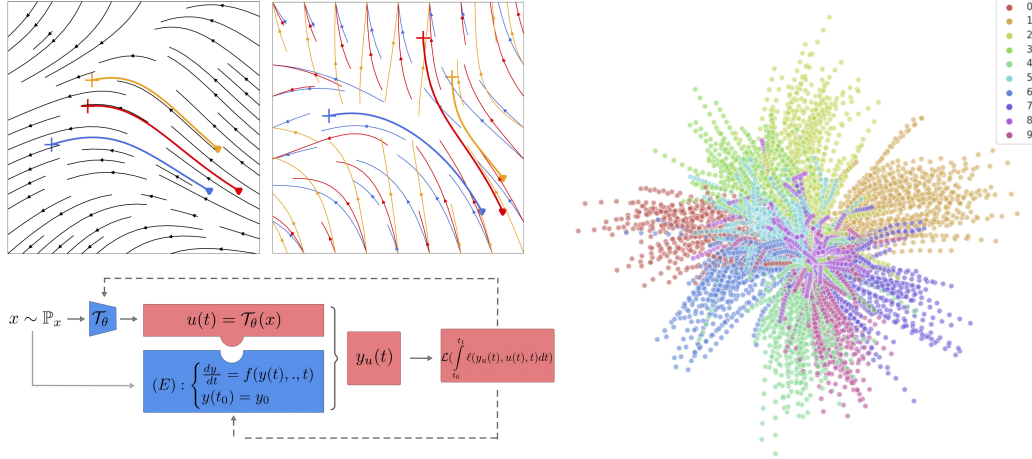


Figure 1: **Upper left:** Idealized dynamical computations of neural modules governed by ODEs and interpreted as particle trajectories in a vector field over time (from triangle to cross.) (*Left*) A standard setting where a single optimal ODE (in black) is learned and integrated for different initial conditions (blue, orange and red). (*Right*) We propose to learn a conditional distribution of *controls* that adjust the dynamical system for every data point. **Lower left:** Diagram of the proposed method. A control variable u is inferred from the data distribution $x \sim \mathbb{P}_x$ thanks to a transformation \mathcal{T}_θ . The control shapes the evolution of the dynamic $y_u(t)$ within the generic class of differential systems following (E) (possibly conditioned by the data itself) for every data point. We rewrite the minimization of the objective function as a Problem of Lagrange, where the integrand ℓ is a function of the controlled dynamic and possibly of the control itself (in the case of control regularization). Minimization of the objective function \mathcal{L} over the data distribution is performed using gradient descent on the parameters of the neural modules (shown in blue), with gradients estimated using the adjoint sensitivity method. Feedforward flow is depicted as plain arrows and back-propagation as dotted arrows. **Right:** t-SNE visualization of learned latent trajectories over time for reconstruction of MNIST digits with AutoencODE.

We argue that this single-dynamics formulation is limited in expressivity [9] and leads to highly complex dynamics straining ODE solvers [10]. As a remedy, we propose a reinterpretation of neural ODE module optimization as an optimal control problem, showing that it is possible to learn a data-conditional distribution of continuous control over the underlying neural dynamical system. We do so by learning a functional mapping from a datum to a corresponding control variable that optimally shapes the evolution of the differential equation. Akin to Neural ODE models, we leverage well-known results in continuous optimal control theory to prove convergence of our method. We discuss its computational efficiency and apply it in the original context of unsupervised image auto-encoding. The contributions of this work are the following:

- We propose a new method for training dynamical neural networks, by augmenting them with a control inference mechanism; this empirically leads to simpler dynamics, faster solver integration, and increases the set of functions the model can express.
- We derive a gradient-based optimization algorithm, reformulating the classic statistical risk minimization as a control Problem of Lagrange [11] for learning a conditional distribution of controls, and prove its convergence.
- We demonstrate the effectiveness of the resulting method in an unsupervised learning application: the proposed *AutoencODE* model learns good representations of natural images, and achieves substantial gains both in clustering accuracy and in image reconstruction quality over baseline auto-encoders.
- We further describe a strategy for sampling data from the latent code distribution and show that it describe a trade-off between image generation quality on CIFAR-10 and data overfitting.

2 Related work

The present work adds to a growing body of literature connecting deep learning models and dynamical systems. For instance, residual networks [12] have been interpreted as discretizations of an ODE [4, 13]. Deep learning optimization has also been reformulated as an optimal control problem [14–16] as an alternative to standard gradient-based learning methods – providing strong error control and convergence results. Of particular interest is the *mean-field optimal control* formulation of [17], which notes the dependence of an unique control variable governing the network dynamics on the whole data population.

This work also builds on the recent development of Neural ODEs, which have already shown great promise for building generative normalizing flows [18] such as for modeling molecular interactions [19] or in mean field games [20]. More recent work has focused on the topological properties of these models [9], the development of novel regularization methods using optimal transport [10], and their adaptation to stochastic differential equations [21].

Finally, this work is also related to network architectures with adaptive weights such as hypernetworks [22], dynamic filters [23] and spatial transformers [24]. Though not explicitly formulated as optimal neural control, these approaches effectively implement a form of dynamic control that modulates neural network activity as a function of input data and feature activations. These results demonstrate, in our opinion, the significant untapped potential value in developing general optimal control methods for deep learning.

3 Background

We start by describing a general formulation of a *controlled* dynamical system whose evolution is ruled by the following differential equation:

$$(E) \quad : \quad \begin{cases} \dot{y}(t) = f(y(t), u(t), t) \\ y(t_0) = y_0 \end{cases}, \quad (1)$$

where $t \in [t_0, t_1]$ is time, $y : t \mapsto \mathbb{R}^n$ is the *state variable*, and $u : t \mapsto u(t)$ is the *control variable* such that $u(t) \in \mathcal{U} \subset \mathbb{R}^p$ is a function belonging to the set of continuous functions $\mathcal{C}^0([t_0, t_1], \mathcal{U})$ hereafter denoted the set of *admissible controls* \mathcal{U} . Given these definitions, we can recall the following lemma:

Lemma 1 - Let f be continuously differentiable with respect to y and u , and continuous with respect to t . Then, for all $u \in \mathcal{C}^0([t_0, t_1], \mathcal{U})$ and for all initial conditions $y(t_0) = y_0$, there exists a unique solution y_u for Eq. (1), called the *controlled state* of the system.

This lemma is a corollary to the Cauchy-Lipschitz theorem which, given sufficient regularity of functions f and u , assures the existence and uniqueness of a solution y_u to Eq. (1) for the control variable u . The main motivation behind our work is to build on this well-defined form of y_u with respect to u in order to “steer” the evolution of the system in an optimal way with respect to each input.

Arguably, the definition in (1) is very general as it encompasses the continuous-time limit formulations of both feedforward ResNets and recurrent neural networks (RNN) architectures (see SI Sec.1). For instance, the kernel weights W and bias β parameterizing a ResNet convolution layer can be interpreted as controls of a discretization of the controlled state $y_u(t)$. In this case, the control variable u represents the set of learned weights of the model that is constant with respect to time and input data.

4 Proposed approach

Considering the simple but ubiquitous framework described by equation (1), we can now draw an interesting parallel with optimal control theory that addresses the problem of determining, within a certain function space, a control u that minimizes a cost ℓ depending on both u and y_u , the unique *controlled state* solution of Eq. (1) guaranteed by Lemma 1. For instance, given some data x following

the distribution \mathbb{P}_x over the space X , one class of problem involves a Lagrangian cost:

$$(\mathcal{P}_\ell) \quad \inf_{u \in \mathbb{U} \subset \mathcal{C}^0([t_0, t_1], \mathcal{U})} \int_{t_0}^{t_1} \ell(x, y_u(t), u(t), t) dt \quad (2)$$

By holding the control variable u constant over time, and assuming existence of a minimum, we can interpret a classic risk-minimization problem of a dynamical neural network in the continuous-time limit as a problem of the following form:

$$(\mathcal{P}_1) \quad \min_{u \in \mathbb{U}} \mathbb{E}_{x \sim \mathbb{P}_x} \left[\int_{t_0}^{t_1} \ell(x, y_u(t), u) dt \right] = \min_{u \in \mathbb{U}} \mathbb{E}_{x \sim \mathbb{P}_x} [\mathcal{L}(x, y_u(t_1), u)], \quad (3)$$

where we simplified the expression by assuming that the objective function only depends on the last system state $y_u(t_1)$ and not on time t . In this case, the variable u is optimized globally over the whole distribution of input data. Note that this formulation also encompasses regularization methods as the function \mathcal{L} can potentially penalize the form of u . We show that several classic objective functions can be formulated as (3) in the SI, but we argue that such a definition presents two shortcomings, as the control variable u is "static" in two ways: **(i)** It is fixed over the data distribution \mathbb{P}_x as the parametrization governing the evolution of the differential system is learned as a constant minimizer. Hence the same dynamical system is applied to all the points of the dataset. This is problematic as ODE flows are homeomorphic transformations of the input space, preserving dataset topology. Hence, they can only continuously deform the space and might struggle to separate complex features space regions with a single differential equation parametrization (Fig. 2). **(ii)** It is fixed over time, as the control variable is actually not dependent on t , which might however add another degree of freedom to the model transformation by describing a time-dependant vector field.

Hence, we are motivated to build models able to perform a dynamic inference of the *control variable* u that will optimally shape y_u trajectory with respect to every feature point. We start from the formulation of a class of differential system as in (1) that represents prior knowledge on the feature transformations that a neural system should describe, and a cost function formulated as (3). We want to learn a mapping $\mathcal{T}_\theta : X \mapsto \mathbb{U} \subset \mathcal{C}^0([t_0, t_1], \mathcal{U})$ that minimizes (\mathcal{P}_1) for every x in the data distribution. In other words, we map an input datum to a controlled state that is optimal with respect to the underlying cost function. More formally, this amounts to learning a conditional probability measure on the space (\mathbb{U}, Υ) of control variables u denoted \mathbb{P}_u^θ such that $\forall U \in \Upsilon, \mathbb{P}_u^\theta(U) = \int \mathbb{1}_{[\mathcal{T}_\theta(x) \in U]} \mathbb{P}_x$, where \mathcal{T}_θ is a transformation from x to u parameterized by θ that we will optimize with respect to the following objective function.

$$(\mathcal{P}_2) \quad \min_{\theta \in \Theta} \mathbb{E}_{(x, u) \sim \mathbb{P}_x \times \mathbb{P}_u^\theta(\cdot|x)} \left[\int_{t_0}^{t_1} \ell(x, y_u(t), u(t)) dt \right] \quad (4)$$

In order to optimize this objective function, we borrow Pontryagin's Maximum Principle [7] from optimal control theory, similarly to [14] and [6], which gives necessary conditions for optimality of Eq. (2) in the form of the minimization of the following Hamiltonian function:

Definition 1 - We denote by (\mathcal{P}_ℓ) the Hamiltonian of the system, the function $\mathcal{H} : X \times \mathbb{R}^n \times \mathbb{U} \times \mathbb{R}^n \times [t_0, t_1] \mapsto \mathbb{R}$ defined as

$$\mathcal{H}(x, y, u, p, t) = p^T f(y, u, t) + \ell(x, y, u, t) \quad (5)$$

Theorem 1 - Pontryagin Maximum Principle (PMP) Let f and ℓ be \mathcal{C}^1 with respect to y and u , and \mathcal{C}^0 with respect to $t, x \in X$. If u^* is an optimal control of (\mathcal{P}_ℓ) , then, denoting $y^* = y_{u^*}$, the associated controlled state, there exists $p^* \in \mathcal{C}^0([t_0, t_1], \mathbb{R}^N)$ such that:

$$\begin{cases} \forall t \in [t_0, t_1], & \mathcal{H}(x, y^*(t), u^*(t), p(t), t) = \inf_{u \in \mathbb{U}} \mathcal{H}(x, y^*(t), u, p, t) \\ \dot{y}^*(t) = \partial_p \mathcal{H}(x, y^*(t), u^*(t), p, t) \text{ and } y^*(t_0) = y_0 \\ \dot{p}^*(t) = -\partial_y \mathcal{H}(x, y^*(t), u^*(t), p, t) \text{ and } p^*(t_1) = 0 \end{cases} \quad (6)$$

The PMP gives necessary conditions for u to be an optimal control of the problem (\mathcal{P}_ℓ) . As pointed out in [14], it can be regarded as a functional expansion of the Karush-Kuhn-Tucker conditions for optimality in non-linear problems constrained by (1). It makes only mild assumptions on the control space \mathbb{U} and even applies f which are non-smooth in u as well as discrete \mathbb{U} . However, since we want

to differentiate the criteria with respect to the control u , we place ourselves in the case of a convex compact set of functions $\mathbb{U} \subset C^0([t_0, t_1], \mathcal{U})$ described by the differentiable transformation \mathcal{T}_θ . We combine the adjoint method for solving the differential system backwards in time with gradient descent for iteratively updating the parameters θ in (\mathcal{P}_2) . The general method is summarized in Algorithm 1 below, with Theorem 2 ensuring the convergence of the method (proof in SI).

4.1 Algorithm for control inference

Algorithm 1: Parametrized control gradient descent

Result: Weights $\{\theta\}$ of function \mathcal{T}_θ

Initialize $\theta_0 \in \Theta$

while *Stopping criterion is False* **do**

- **Sample** batch from data: $(x_i)_{i \in B} \sim \mathbb{P}_x$

- **Evaluate:** $u_i \leftarrow T_{\theta^k}(x_i)$

- **Solve** the batch-augmented direct equation:

$$(\mathcal{S}_1) : (y_{u_i})_{i \in B} = \begin{cases} \dot{y}(t) = f(y(t), u_i(t), t) & \forall i \in B \\ y(t_0) = y_0 \end{cases}$$

- **Solve** the relative adjoint equation:

$$(\mathcal{S}_2) : (p_{u_i})_{i \in B} = \begin{cases} \dot{p}(t) = -\partial_y \mathcal{H}(x_i, y_{u_i}(t), u_i(t), p(t), t) & \forall i \in B \\ p(t_1) = 0 \end{cases}$$

- **Set:** $\mathcal{H}_i = \mathcal{H}(y_{u_i}(t), u_i(t), p_i(t), t)$

- **Differentiate** \mathcal{H}_i with respect to u .

- **Compute** Chain rule:

$$\forall i \in B, \quad \frac{\partial \mathcal{H}}{\partial \theta}(x_i, y_{u_i}(t_1), u_i(t_1), p_{u_i}(t_1), t_1) = \frac{\partial u}{\partial \theta} \cdot \frac{\partial \mathcal{H}}{\partial u}(x_i, y_{u_i}(t_1), u_i(t_1), p_{u_i}(t_1), t_1)$$

- **Compute** gradient update:

$$\theta^{k+1} = \text{update}(\theta^k, \lambda, \frac{1}{|B|} \sum_{i \in B} \frac{\partial \mathcal{H}}{\partial \theta}(y_{u_i}(t_1), u_i(t_1), p_{u_i}(t_1), t_1))$$

- **Increment:** $k = k + 1$

end

Note 1 - Mini-batch We present a mini-batch version of the training algorithm by concatenating the states of several differential equations together to speed up training and improve gradient estimates. Although this technique might increase the number solver evaluations for the combined system in certain cases, it did not increase substantially in our experiments, as observed in [6].

Note 2 - Multiple gradient estimates It is possible to differentiate with respect to multiple points in time similar to [6] in order to penalize different states of the system. Note that, in our definition, the cost function ℓ can support new forms of regularization of the dynamics such as for instance a continuous regularization on the whole integration segment.

Theorem 2 - Convergence of parameterized control gradient descent: Let $m \in \mathbb{N}$ and let f and ℓ be C^1 functions with respect to y and C^0 with respect to t . Suppose ℓ has an L -Lipschitz gradient with respect to y and that f is L -Lipschitz in y . Let $\Theta = \mathbb{R}^n$ be the space of real-valued parameters of the θ -parameterized function $\mathcal{T}_\theta : x \mapsto \mathbb{U} \subset C^0([t_0, t_1], \mathcal{U})$ is L -Lipschitz continuous in θ . Then, there exists a sequence of non-negative step size $(\lambda_k)_{k \in \mathbb{N}}$ such that the sequence (θ^k) defined in Algorithm 1 converges almost surely to the set of zeros $\{\theta^*\} \subset \Theta$ of the operator $\theta \mapsto \frac{1}{m} \sum_{i=1}^m \nabla_\theta \mathcal{H}(x_i, y_{\mathcal{T}_\theta(x_i)}(t_1), u_{\mathcal{T}_\theta(x_i)}(t_1), p(t_1), t_1)$ where, $y_{\mathcal{T}_\theta(x)}$ is the controlled state of the ordinary differential problem (1).

5 Experimental results

5.1 Supervised classification on a toy example

We first evaluate the proposed method on a toy classification problem following [9, 25]. Specifically, we learn a mapping function from \mathbb{R}^2 to the label set $\{0, 1\}$ with a single ODE transformation layer followed by a linear classification layer. We define a class of ODE flows $f(x, y_u(t), u(t), t)$ acting on \mathcal{R}^2 in the form of a three-layer MLP. The control $u(t) = u$ is here constant and represents the model parameters inferred by a second MLP network (see SI). We train the weights of this second

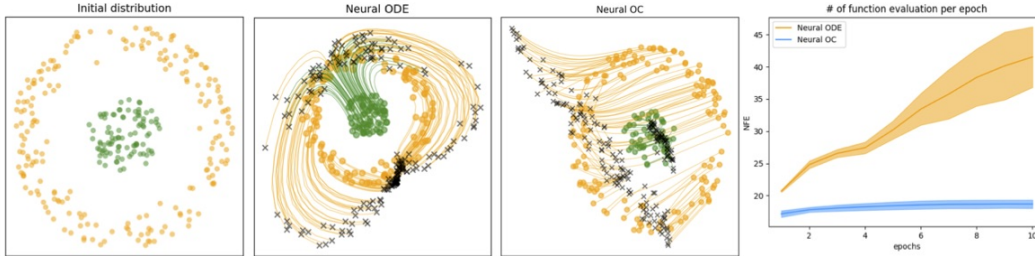


Figure 2: Classification of the annulus dataset. (1) Initial disposition of the data distribution. (2) Trajectories learned with Neural ODEs. The model struggle to tear apart the connected region in orange to linearly separate the two classes. (3) Trajectories learned with the neural control. (4) Average number of function evaluations (NFE) called by the solver for 10 epochs over 10 different initializations.

model with categorical cross-entropy, such that the final representations $y_u(t_1)$ must linearly separate the classes on the annulus dataset (see Fig. 2).

As stated in [9], Neural ODE transformations are homeomorphic and, hence, preserve the topology of the space, notably the linking number of data manifolds, which might lead to unstable and complex flows for intricate data manifold – possibly requiring a very large number of evaluation steps (NFE) for solving the Eq. [6, 18]. In comparison, our proposed method is not affected by this problem, as every trajectory belongs to its own specific flow, thus breaking the topological constraint of these transformations and allowing for simpler paths reducing the cost of solving the system (Fig. 2).

5.2 Unsupervised learning of image representation

We now describe cast our approach in the form of an auto-encoding model for low-dimensional representation learning. Our idea is to invoke a very standard class of ordinary differential equations to "encode" the model's latent representations as the state of the differential equation at a fixed point in time. We slightly simplify the convolution architecture tested in [26, 27] and apply batch normalization to all layers (see SI). We replace the encoder final linear projection that maps the feature activation tensor from convolutional layers to the low-dimensional euclidean latent space by a projection on a real-valued parametrization space of the control function u such that the encoder part reads:

$$\begin{aligned} \mathcal{T}_\theta : X &\mapsto M_{n,n}(\mathbb{R}) \\ x &\mapsto T_\theta(x) = (u_{i,j})_{1 \leq i,j \leq n} \end{aligned} \quad (7)$$

The latent code of the model is "read" as the solution of a simple linear homogeneous differential system controlled by the control coefficients $(u_{i,j})_{1 \leq i,j \leq n}$ with constant initial condition y_0 randomly initialized in $[0; 1]$:

$$\begin{cases} \dot{y}_u^i(t) = \sum_{j=1}^n u_{i,j} y_u^j(t) \quad \forall i \in \{1, \dots, n\} \\ y(t_0) = y_0 \end{cases} \quad (8)$$

Intuitively, this can be interpreted as learning a mapping from the input image to a vector field \mathcal{X} on the latent space, such that the system trajectory is oriented toward a good reconstruction of x at a fixed time $t = t_1$. We make no additional change to the decoder. Because the latent representation of our auto-encoding model is intrinsically defined by the evolution of an ordinary differential equation, we call the system **AutoencODE**. We train the parameters of the encoder and decoder module for minimizing the mean-squared error (MSE) on CIFAR-10 [28] and

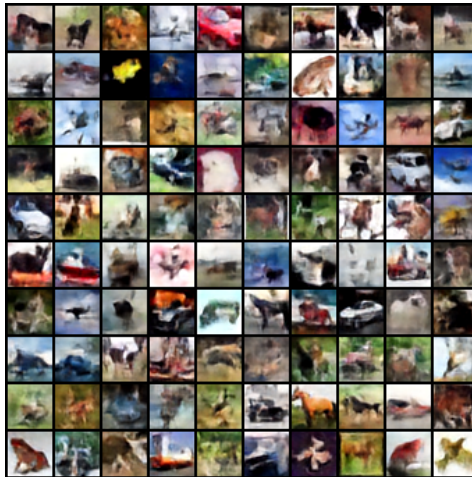


Figure 3: Random samples generated with **AutoencODE** trained on CIFAR-10 from a Gaussian Mixture Model with 5000 components.



Figure 4: Left to right: Temporal evolutions of an image reconstruction along controlled *orbits* of **AutoencODE** for representative CIFAR-10 and CelebA test images. Last column: ground truth image.

CelebA [29] or alternatively the Kullback-Leibler divergence between the data distribution and the output of the decoder for MNIST [30] (formulas in SI.) Gradient descent is performed for 50 epochs with the Adam [31] optimizer with learning rate $\lambda = 1e^{-3}$ reduced by half every time the loss plateaus. All experiments are run on a single GPU GeForce Titan X with 12 GB of memory.

FID		
Model	CIFAR-10	CelebA (64x64)
Variational Bayes AE [†] [32]	105.45	68.07
Auto-encoder [†] (100 components)	73.24	63.11
PixelCNN [33]	65.93	-
Auto-encoder [†] (1000 components)	55.55	55.60
DCGAN [34]	37.11	-
EBM (10 hist. ensemble) [35]	38.2	-
MoLM [36]	33.8	-
Auto-encoder [†] (10000 components)	32.83	53.32
NCSN [37]	25.32	-
SNGAN [38]	21.7	-
AutoGAN [39]	12.42	-
AutoencODE (100 components)	34.90	55.27
AutoencODE (1000 components)	24.19	52.47
AutoencODE (10000 components)	11.39	46.45

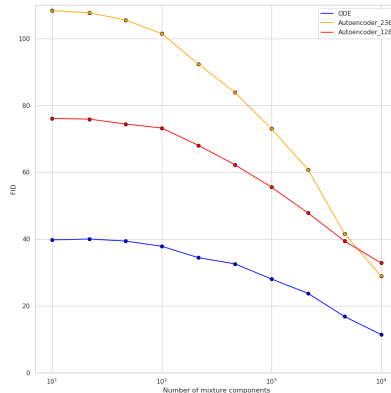


Figure 5: **Left:** Frechet Inception Distance (FID) for several recent architectures. (lower is better, best models in bold. Models that are evaluated using authors code are noted with [†]. CelebA results are given for our implementations only as data processing is inconsistent across models.) **Right:** Evolution of FID as a function of the number of components in the Gaussian mixture used to fit the latent distribution. We also test an autoencoder with twice the capacity (236-dimensional), exactly matching the number of parameters of our model. Interestingly, this model performs worst under a low component regime. We interpret this as a manifestation of the "curse of dimensionality", as the latent examples population becomes less dense in this augmented space, making the naive gaussian mixture fitting less accurate to fit the latent distribution.

We acknowledge that the dynamics in Eq. (8) are fairly simple and that our control variable u differs slightly from our general formulation in the sense that it is constant over time. Additionally, since the

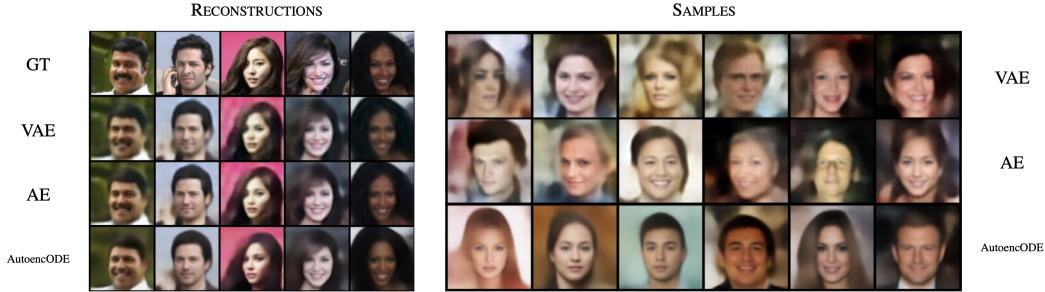


Figure 6: **Left** Reconstructions of random test images from CelebA for different autoencoding models. **Right**: Random samples from the latent space. Deterministic models are fitted with a 100 components GMM.

output dimension of the encoder grows quadratically with the desired latent code dimension of the bottleneck, we adopt a sparse prediction strategy to avoid memory limitation due to the linear layer, where as few as two elements of each row of $(u_{i,j})_{1 \leq i,j \leq n}$ are non-zero. We believe that the increase in representational power over a vanilla Autoencoder, as shown by the unsupervised classification and FID improvements, despite these simplistic assumptions, shows the great potential of this approach for representation learning.

5.3 Image generation

In order to endow our deterministic model with the ability to generate image samples, we perform, similarly to [26], an ex-post density estimation of the distribution of the latent trajectories final state. Namely, we employ a gaussian mixture model (GMM) fitted with Expectation-Maximization, and explore the effect of increasing the number of components in the mixture. We report in Fig.5, contrary to [26], a substantial decrease of the Frechet Inception Distance (FID, [40]) of our sampled images to the image test set with increasing number of components in the mixture. These results suggest, considering the identical architecture of the encoder and decoder to a vanilla model, that the optimal encoding control formulation produced a structural change in the latent manifold organization. We further show that our approach compares favorably over recent generative techniques (see Fig.5). Finally, we note that this model offers several original possibilities to explore, such as sampling from the control coefficients, or adding a regularization on the dynamic evolution as in [10], which we leave for future work.

5.4 Unsupervised image classification

Clustering accuracy		
Model	CIFAR-10	MNIST
K-means [41]	22.9	57.2
Spectral clustering [42]	24.7	69.6
Variational Bayes AE [†] [32]	29.1	83.2
Sparse AE [43]	29.7	82.7
Denoising AE [44]	29.7	83.2
AE (GMM) [†]	31.4	81.2
GAN (2015) [34]	31.5	82.8
DeepCluster [45]	37.4	65.6
DAC [46]	52.2	97.8
IIC [47]	61.7	99.2
AutoencODE (GMM) [†]	33.31	86.02
AutoencODE (t-SNE + GMM) [†]	27.00	97.26

Figure 7: Unsupervised image clustering accuracy on CIFAR-10 and MNIST against recent models. Results obtained with the authors original code are noted with [†].

We further investigate the representations learned by our model by measuring its clustering accuracy against several other techniques in Fig. 7. Similarly to the image generation experiment, we consider the final state of the dynamical system as the latent representation that we cluster using a 10 component mixture. We do not perform any supplementary fine-tuning nor data augmentation to train our model, but we also test a version with further dimensionality reduction using t-SNE [48]. The results, although inferior to specific recent deep clustering techniques, show better clustering accuracy than other autoencoding models, suggesting again a different organization of the latent code compared to the vanilla linear projection.

6 Conclusion

In this work, we have presented an original modulation system for continuous-time neural feature transformations that theoretically relates to optimal control. We have shown that it is possible to dynamically shape the trajectories of the transformation module applied to the data, by augmenting the network with a trained control inference mechanism, and further demonstrated that this can be applied in the context of unsupervised image representation learning. In future work, we would like to investigate the robustness and generalization properties of such controlled models as well as their similarities with fast-synaptic modulation systems observed in neuroscience, and test this on natural applications such as recurrent neural networks and robotics.

Broader Impact

The development of artificial neural systems that are both functionally expressive and context-adaptable could bring new insights to brain sciences and other computational fields. We hope that this original formulation is a contribution in this direction. Our particular focus of generative modeling is itself a valuable field of research that finds potential applications in medicine, education and art. We also believe that the continuous-time approach outlined here could be potentially quite useful for computational neuroscience modeling, where controlled neural dynamics as a function of input stimulus is a well-studied phenomenon. To help foster collaboration with this and related disciplines we have released an open-source version of our code.

References

- [1] Izhikevich, E.: *Dynamical Systems in Neuroscience: The Geometry of Excitability and Bursting*. Massachusetts: The MIT Press (2007)
- [2] Weinan, W.: A proposal on machine learning via dynamical systems. *Communications in Mathematics and Statistics* **5**(1) (March 2017)
- [3] Haber, E., Ruthotto, L.: Stable architectures for deep neural networks. *Inverse Problems* **34**(1) (Dec 2017) 014004
- [4] Ruthotto, L., Haber, E.: Deep neural networks motivated by partial differential equations (2018)
- [5] D., S.: Neural circuits as computational dynamical systems. *Curr Opin Neurobiol.* **25** (2014) 156-163
- [6] Chen, R.T.Q., Rubanova, Y., Bettencourt, J., Duvenaud, D.: Neural ordinary differential equations (2018)
- [7] Pontryagin, Lev Semenovich ; Boltyanskii, V.G..G.R.V..M.E.F.: *The mathematical theory of optimal processes*. (1962)
- [8] Breakspear, M.: Dynamic models of large-scale brain activity. *Nature Neuroscience* **20**(3) (2017) 340–352
- [9] Dupont, E., Doucet, A., Teh, Y.W.: Augmented neural odes (2019)
- [10] Finlay, C., Jacobsen, J.H., Nurbekyan, L., Oberman, A.M.: How to train your neural ode: the world of jacobian and kinetic regularization (2020)
- [11] Evans, L.C.: *An introduction to mathematical optimal control theory version 0.2*
- [12] He, K., Zhang, X., Ren, S., Sun, J.: Deep residual learning for image recognition (2015)
- [13] Chang, B., Meng, L., Haber, E., Ruthotto, L., Begert, D., Holtham, E.: Reversible architectures for arbitrarily deep residual neural networks (2017)
- [14] Li, Q., Chen, L., Tai, C., E, W.: Maximum principle based algorithms for deep learning (2017)
- [15] Benning, M., Celledoni, E., Ehrhardt, M.J., Owren, B., Schönlieb, C.B.: Deep learning as optimal control problems: models and numerical methods (2019)
- [16] Liu, G.H., Theodorou, E.A.: Deep learning theory review: An optimal control and dynamical systems perspective (2019)
- [17] E, W., Han, J., Li, Q.: A mean-field optimal control formulation of deep learning (2018)
- [18] Grathwohl, W., Chen, R.T.Q., Bettencourt, J., Sutskever, I., Duvenaud, D.: Ffjord: Free-form continuous dynamics for scalable reversible generative models (2018)
- [19] Köhler, J., Klein, L., Noé, F.: Equivariant flows: sampling configurations for multi-body systems with symmetric energies (2019)

- [20] Ruthotto, L., Osher, S., Li, W., Nurbekyan, L., Fung, S.W.: A machine learning framework for solving high-dimensional mean field game and mean field control problems (2019)
- [21] Tzen, B., Raginsky, M.: Neural stochastic differential equations: Deep latent gaussian models in the diffusion limit (2019)
- [22] Ha, D., Dai, A., Le, Q.V.: Hypernetworks (2016)
- [23] Brabandere, B.D., Jia, X., Tuytelaars, T., Gool, L.V.: Dynamic filter networks (2016)
- [24] Jaderberg, M., Simonyan, K., Zisserman, A., Kavukcuoglu, K.: Spatial transformer networks (2015)
- [25] Lin, H., Jegelka, S.: Resnet with one-neuron hidden layers is a universal approximator (2018)
- [26] Ghosh, P., Sajjadi, M.S.M., Vergari, A., Black, M., Schölkopf, B.: From variational to deterministic autoencoders (2019)
- [27] Tolstikhin, I., Bousquet, O., Gelly, S., Schoelkopf, B.: Wasserstein auto-encoders (2017)
- [28] Krizhevsky, A.: Learning multiple layers of features from tiny images. University of Toronto (05 2012)
- [29] Liu, Z., Luo, P., Wang, X., Tang, X.: Deep learning face attributes in the wild. In: Proceedings of International Conference on Computer Vision (ICCV). (December 2015)
- [30] Y. LeCun, L. Bottou, Y.B., Haffner., P.: "gradient-based learning applied to document recognition." Proceedings of the IEEE (1998)
- [31] Kingma, D.P., Ba, J.: Adam: A method for stochastic optimization (2014)
- [32] Kingma, D.P., Welling, M.: Auto-encoding variational bayes (2013)
- [33] van den Oord, A., Kalchbrenner, N., Vinyals, O., Espeholt, L., Graves, A., Kavukcuoglu, K.: Conditional image generation with pixelcnn decoders (2016)
- [34] Radford, A., Metz, L., Chintala, S.: Unsupervised representation learning with deep convolutional generative adversarial networks (2015)
- [35] Du, Y., Mordatch, I.: Implicit generation and generalization in energy-based models (2019)
- [36] Ravuri, S., Mohamed, S., Rosca, M., Vinyals, O.: Learning implicit generative models with the method of learned moments (2018)
- [37] Song, Y., Ermon, S.: Generative modeling by estimating gradients of the data distribution (2019)
- [38] Miyato, T., Kataoka, T., Koyama, M., Yoshida, Y.: Spectral normalization for generative adversarial networks (2018)
- [39] Gong, X., Chang, S., Jiang, Y., Wang, Z.: Autogan: Neural architecture search for generative adversarial networks (2019)
- [40] Heusel, M., Ramsauer, H., Unterthiner, T., Nessler, B., Hochreiter, S.: Gans trained by a two time-scale update rule converge to a local nash equilibrium (2017)
- [41] Lloyd, S.P.: Least squares quantization in pcm. IEEE Transactions on Information Theory **28** (1982) 129–137
- [42] Shi, J., Malik, J.: Normalized cuts and image segmentation. Technical report (2000)
- [43] Ng, A.: Sparse autoencoders (2011)
- [44] Vincent, P., Larochelle, H., Lajoie, I., Bengio, Y., Manzagol, P.A.: Stacked denoising autoencoders: Learning useful representations in a deep network with a local denoising criterion. J. Mach. Learn. Res. **11** (December 2010) 3371–3408
- [45] Caron, M., Bojanowski, P., Joulin, A., Douze, M.: Deep clustering for unsupervised learning of visual features (2018)
- [46] Chang, J., Wang, L., Meng, G., Xiang, S., Pan, C.: Deep adaptive image clustering. In: 2017 IEEE International Conference on Computer Vision (ICCV). (2017) 5880–5888
- [47] Ji, X., Henriques, J.F., Vedaldi, A.: Invariant information clustering for unsupervised image classification and segmentation (2018)
- [48] Maaten, L.v.d., Hinton, G.: Visualizing data using t-sne. Journal of machine learning research **9**(Nov) (2008) 2579–2605
- [49] Dempster, A.P., Laird, N.M., Rubin, D.B.: Maximum likelihood from incomplete data via the em algorithm. Journal of the Royal Statistical Society. Series B (Methodological) **39**(1) (1977) 1–38

Supplementary information

G Examples of continuous-time neural transformation

G.1 Recurrent Neural Networks

A standard formulation of a RNN cell computation scheme is a discretized version of Eq.1 where $y(t)$ represents the “hidden state” of the cell and f represents the update equation applied by this cell at every time step. We can absorb the time-varying data information stream $x(t)$ and gating mechanism $\epsilon(\cdot)$ into the definition of f in Eq.1, so that

$$(RNN \text{ evolution}) : \begin{cases} \dot{y}(t) = \sigma \left(\epsilon(y(t)) [W_y * y(t) + \beta_1] + (1 - \epsilon(y(t))) [W_x * x(t) + \beta_2] \right) \\ y(t_0) = y_0 \end{cases}, \quad (9)$$

where $*$ denotes the convolution operation, W_y, W_x are the convolution kernels respectively applied to the hidden state and data, and β_1, β_2 are biases. We note that, in this formulation, f actually depends on x , which slightly changes the notation of section 3 and 4.

G.2 Residual Neural Networks

The similarity between the forward computation of Residual Networks [12] and the discretized Euler integration of the following ordinary differential equation have been explored in [3] and [6] where the continuous-time update equation of a residual convolution layer of a ResNet reads

$$(ResNet \text{ evolution}) : \begin{cases} \dot{y}(t) = W_y * y(t) + \beta \\ y(t_0) = x(0) \end{cases}. \quad (10)$$

In those two examples, the convolution kernel W and bias β parameterizing the convolution transformations can be interpreted as controls (of a discretization) of the controlled state $y_{W,\beta}(t)$. In this case, the control variable represents the set of learned weights of the model that is constant with respect to time and input data.

H Proof of Theorem 2

Theorem 2 - Convergence of parameterized control gradient descent (final version) Let $m \in \mathbb{N}$ and let f and ℓ be \mathcal{C}^1 functions with respect to y and \mathcal{C}^0 with respect to t . Suppose ℓ has an L -Lipschitz gradient with respect to y and that f is L -Lipschitz in y . Let $\Theta = \mathbb{R}^n$ be the space of real-valued parameters of the θ -parameterized function $\mathcal{T}_\theta : x \mapsto \mathcal{U} \subset \mathcal{C}^0([t_0, t_1], \mathcal{U})$ is L -Lipschitz continuous in θ . Then, there exists a sequence of non-negative step size $(\lambda_k)_{k \in \mathbb{N}}$ such that the sequence (θ^k) defined in Algorithm 1 converges almost surely to the set of zeros $\{\theta^*\} \subset \Theta$ of the operator $\theta \mapsto \frac{1}{m} \sum_{i=1}^m \nabla_\theta \mathcal{H}(x_i, y_{\mathcal{T}_\theta(x_i)}(t_1), u_{\mathcal{T}_\theta(x_i)}(t_1), p(t_1), t_1)$ where, $y_{\mathcal{T}_\theta(x)}$ is the controlled state of the ordinary differential problem.

For readability, let us rewrite, for all $\theta \in \Theta$ and $t \in [t_0, t_1]$, the expression $\mathcal{T}_{\theta(x)}(t)$ as $\mathcal{T}(\theta, x, t)$, and $y_{\mathcal{T}_\theta(x)}(t)$ as $y(\theta, x, t)$. Similarly, for all $p \in \mathcal{C}^0([t_0, t_1])$ that are solutions of the PMP third condition in equation (6), we rewrite $p(t) = p(\theta, t)$ to make explicit the dependence of the adjoint ODE on θ .

To prove our result, we will use the following lemma taken from [Mairal, 2013, Lemma A.5]:

Lemma 1: Let $(a^k)_{k \in \mathbb{N}^+}, (b^k)_{k \in \mathbb{N}^+}$ be two nonnegative real sequences. Assume that $\sum_{k \in \mathbb{N}^+} a^k b^k$ converges and $\sum_{k \in \mathbb{N}^+} a^k$ diverges, and there exists $K \geq 0$ such that $|b^{k+1} - b^k| \leq K a^k$. Then b^k converges to 0.

We consider the sequence $(\theta^k)_{k \in \mathbb{N}}$ built by Algorithm 1 and the following operator:

$$\begin{cases} H : \Theta \mapsto \mathbb{R} \\ \theta \mapsto H(\theta) = \frac{1}{m} \sum_{i=1}^m \mathcal{H}(x_i, y(\theta, x_i, t_1), \mathcal{T}(\theta, x_i, t_1), p(\theta, t_1), t_1) \end{cases}$$

We want to show, assuming a stochastic sampling method yielding an unbiased gradient estimator of H as in Algorithm 1, that the sequence converges almost surely to the set of fixed point of H .

First, from the PMP third condition stated in equation (6), we have that $\forall \theta \in \Theta, p(\theta, t_1) = 0$. Hence, we can write:

$$\forall \theta \in \Theta, \quad H(\theta) = \frac{1}{m} \sum_{i=1}^m \ell(x_i, y(\theta, x_i, t_1), \mathcal{T}(\theta, x_i, t_1), t_1) \quad (11)$$

Furthermore, from the assumption that for any $x \in \sigma(X)$, the function $u \mapsto \ell(x, y_u(t_1), u(t_1), t_1)$ is bounded from below and L_ℓ -Lipschitz continuous, and that $\theta \mapsto \mathcal{T}(\theta, x, t)$ Lipschitz-continuous, we find:

$$\begin{aligned} \exists H^* \text{ s.t., } \quad & \forall \theta \in \Theta, H(\theta) \geq H^* \\ \exists L_H \text{ s.t., } \quad & \forall (\theta_1, \theta_2) \in \Theta^2, \|H(\theta_1) - H(\theta_2)\| \leq L_H \|\theta_1 - \theta_2\| \end{aligned}$$

Additionally, we show that for any $x \in \sigma(X)$, $\mathcal{H}(x, y(\theta, x, t_1), \mathcal{T}(\theta, x, t_1), p(\theta, t_1), t_1)$ has an L -Lipschitz gradient in θ .

$$\begin{aligned} \forall x \in \sigma(X), \forall (\theta_1, \theta_2) \in \Theta^2, \quad & \|\nabla_{\theta} \mathcal{H}(x, y(\theta_1, x, t_1), \mathcal{T}(\theta_1, x, t_1), p(\theta_1, t_1), t_1) \\ & - \nabla_{\theta} \mathcal{H}(x, y(\theta_2, x, t_1), \mathcal{T}(\theta_2, x, t_1), p(\theta_2, t_1), t_1)\| \\ \leq & \|\nabla_{\theta} [p(\theta_1, t_1)^T f(y(\theta_1, x, t_1), \mathcal{T}(\theta_1, x, t_1), t_1) - p(\theta_2, t_1)^T f(y(\theta_2, x, t_1), \mathcal{T}(\theta_2, x, t_1), t_1)]\| \\ & + \|\nabla_{\theta} [\ell(x, y(\theta_1, x, t_1), \mathcal{T}(\theta_1, x, t_1), t_1) - \ell(x, y(\theta_2, x, t_1), \mathcal{T}(\theta_2, x, t_1), t_1)]\| \end{aligned}$$

Again, given the PMP condition $\forall \theta \in \Theta, p(\theta, t_1) = 0$, we have $\forall \theta \in \Theta, \nabla_{\theta} p(t_1, \theta) = 0$ which allows us to write:

$$\begin{aligned} & \|\nabla_{\theta} \mathcal{H}(x, y(\theta_1, x, t_1), \mathcal{T}(\theta_1, x, t_1), p(\theta_1, t_1), t_1) - \\ & \quad \nabla_{\theta} \mathcal{H}(x, y(\theta_2, x, t_1), \mathcal{T}(\theta_2, x, t_1), p(\theta_2, t_1), t_1)\| \\ \leq & \|\nabla_{\theta} [\ell(x, y(\theta_1, x, t_1), \mathcal{T}(\theta_1, x, t_1), t_1) - \ell(x, y(\theta_2, x, t_1), \mathcal{T}(\theta_2, x, t_1), t_1)]\| \end{aligned}$$

Since ℓ has L -Lipschitz gradient in y , we can write the following inequality:

$$\begin{aligned} & \|\nabla_{\theta} \ell(x, y(\theta_1, x, t_1), \mathcal{T}(\theta_1, x, t_1), t_1) - \nabla_{\theta} \ell(x, y(\theta_2, x, t_1), \mathcal{T}(\theta_2, x, t_1), t_1)\| \\ \leq & L_{\ell} \|y(\theta_1, x, t_1) - y(\theta_2, x, t_1)\| \\ = & L_{\ell} \left\| \int_{t_0}^{t_1} [f(y(\theta_1, x, t), \mathcal{T}(\theta_1, x, t), t) - f(y(\theta_2, x, t), \mathcal{T}(\theta_2, x, t), t)] dt \right\| \end{aligned}$$

Moreover, since f is Lipschitz-continuous in y and continuous in u, t , and y, u are continuous in t , $\exists \tau \in [t_0, t_1]$, s.t:

$$\begin{aligned} & L_{\ell} \left\| \int_{t_0}^{t_1} [f(y(\theta_1, x, t), \mathcal{T}(\theta_1, x, t), t) - f(y(\theta_2, x, t), \mathcal{T}(\theta_2, x, t), t)] dt \right\| \\ \leq & (t_1 - t_0) L_{\ell} \|f(y(\theta_1, x, \tau), \mathcal{T}(\theta_1, x, \tau), \tau) - f(y(\theta_2, x, \tau), \mathcal{T}(\theta_2, x, \tau), \tau)\| \\ \leq & (t_1 - t_0) L_{\ell} L_f \|\mathcal{T}(\theta_1, x, \tau) - \mathcal{T}(\theta_2, x, \tau)\| \end{aligned}$$

Finally, since $\mathcal{T}(\theta, x, \tau)$ is Lipschitz-continuous in θ , we can write:

$$\forall (\theta_1, \theta_2) \in \Theta^2, \forall x \in X, \quad (t_1 - t_0) L_{\ell} L_f \|\mathcal{T}(\theta_1, x, \tau) - \mathcal{T}(\theta_2, x, \tau)\| \leq (t_1 - t_0) L_{\ell} L_f L_{\mathcal{T}} \|\theta_1 - \theta_2\|$$

Hence, given the definition of H we can show the following inequality holds:

$$\forall (\theta_1, \theta_2) \in \Theta^2, \quad \|\nabla_{\theta} H(\theta_1) - \nabla_{\theta} H(\theta_2)\| \leq (t_1 - t_0)L_{\ell}L_fL_{\mathcal{T}}\|\theta_1 - \theta_2\| \quad (12)$$

Let us now denote $(\lambda^k)_{k \in \mathbb{N}}$ the deterministic sequence of positive step-sizes used to update the sequence $(\theta^k)_{k \in \mathbb{N}}$. We further make a standard hypothesis regarding its convergence rate:

$$\sum_{k=1}^{\infty} \lambda^k = \infty \quad \text{and} \quad \sum_{k=1}^{\infty} (\lambda^k)^2 < \infty \quad (13)$$

We denote $\nabla_{\theta} \hat{H}(\theta^k)$ the mini-batch estimation of gradient of H at step k . Given the definition of this operator we can exhibit an upper bound on the gradient estimation error: $\forall k \in \mathbb{N}, \exists \Gamma \geq 0$, such that $\|\nabla_{\theta} \hat{H}(\theta^k) - \nabla_{\theta} H(\theta^k)\| \leq \Gamma$ almost surely. Using [Lemma 1.2.3 from Nesterov, 2003] and letting $\langle \cdot, \cdot \rangle$ denote an inner product on \mathbb{R}^n , we can now write that, $\forall k \in \mathbb{N}$

$$\begin{aligned} H(\theta^{k+1}) &\leq H(\theta^k) + \langle \nabla_{\theta} H(\theta^k), \lambda^k(\theta^{k+1} - \theta^k) \rangle + \frac{(t_1 - t_0)L_{\ell}L_fL_{\mathcal{T}}}{2} \|\lambda^k(\theta^{k+1} - \theta^k)\|^2 \\ &\leq H(\theta^k) + \langle \nabla_{\theta} H(\theta^k), \lambda^k(\nabla_{\theta} H(\theta^k) - \nabla_{\theta} \hat{H}(\theta^k)) \rangle + \langle \nabla_{\theta} H(\theta^k), \lambda^k \nabla_{\theta} H(\theta^k) \rangle \\ &\quad + \frac{(\lambda^k)^2(t_1 - t_0)L_{\ell}L_fL_{\mathcal{T}}}{2} \|\theta^{k+1} - \theta^k\|^2 \end{aligned}$$

Taking the conditional expectation with respect to $(x^i)_{1 \leq i \leq k}$, the sampled vector of data points at steps 1 to $k-1$, and given that our mini-batch estimator is unbiased, it comes that:

$$\begin{aligned} &\mathbb{E} \left[\langle \nabla_{\theta} H(\theta^k), \lambda^k \nabla_{\theta} H(\theta^k) - \lambda^k \nabla_{\theta} \hat{H}(\theta^k) \rangle | x^1, \dots, x^{k-1} \right] \\ &= \langle \nabla_{\theta} H(\theta^k), \lambda^k \nabla_{\theta} H(\theta^k) - \lambda^k \mathbb{E} [\nabla_{\theta} \hat{H}(\theta^k) | x^1, \dots, x^{k-1}] \rangle = 0 \end{aligned}$$

Hence, from Adam's law of total expectation,

$$\mathbb{E}[H(\theta^{k+1})] \leq \mathbb{E}[H(\theta^k)] + \mathbb{E} \left[\langle \nabla_{\theta} H(\theta^k), \lambda^k \nabla_{\theta} H(\theta^k) \rangle \right] + \frac{(t_1 - t_0)L_{\ell}L_fL_{\mathcal{T}}}{2} (\lambda^k)^2 \|\theta^{k+1} - \theta^k\|^2$$

by summing over $k = 1$ to $K \in \mathbb{N}$ and lower-bounding $H(\theta^{K+1})$ with H^* , we obtain the following inequality:

$$\mathbb{E} \left[\sum_{k=1}^K \langle \nabla_{\theta} H(\theta^k), \lambda^k \nabla_{\theta} H(\theta^k) \rangle \right] \leq H(\theta^1) - H^* + \frac{(t_1 - t_0)L_{\ell}L_fL_{\mathcal{T}}}{2} \mathbb{E} \left[\sum_{k=1}^K (\lambda^k)^2 \|\nabla_{\theta} \hat{H}(\theta^k)\|^2 \right]$$

We take the limit of this inequality for $K \mapsto \infty$. Since the terms are non-negative, we can swap expectation and infinite summation:

$$\mathbb{E} \left[\sum_{k=1}^{\infty} \langle \nabla_{\theta} H(\theta^k), \lambda^k \nabla_{\theta} H(\theta^k) \rangle \right] \leq H(\theta^1) - H^* + \frac{(t_1 - t_0)L_{\ell}L_fL_{\mathcal{T}}}{2} \mathbb{E} \left[\sum_{k=1}^{\infty} (\lambda^k)^2 \|\nabla_{\theta} \hat{H}(\theta^k)\|^2 \right]$$

We know that $\|\nabla_{\theta} \hat{H}(\theta^k)\|^2$ converges almost surely to zero and that $\sum_{k=1}^{\infty} (\lambda^k)^2 < \infty$. This allows us to show that $\mathbb{E}[\sum_{k=1}^{\infty} (\lambda^k)^2 \|\nabla_{\theta} \hat{H}(\theta^k)\|^2] < \infty$. Considering the positivity of the sequence, this further lets us state that this series almost surely converges. We finally note the following upper bound, given equation (12) and given that H is L_H -Lipschitz continuous:

$$\begin{aligned} &| \|\nabla_{\theta} H(\theta^{k+1})\|^2 - \|\nabla_{\theta} H(\theta^k)\|^2 | \\ &= (\|\nabla_{\theta} H(\theta^{k+1})\| + \|\nabla_{\theta} H(\theta^k)\|) \cdot \|\nabla_{\theta} H(\theta^{k+1}) - \nabla_{\theta} H(\theta^k)\| \\ &\leq 2L_H(t_1 - t_0)L_{\ell}L_fL_{\mathcal{T}}\|\theta^{k+1} - \theta^k\| \\ &\leq 2L_H(t_1 - t_0)L_{\ell}L_fL_{\mathcal{T}}(\lambda^k)\|\nabla_{\theta} \hat{H}(\theta^k)\| \\ &\leq 2L_H(t_1 - t_0)L_{\ell}L_fL_{\mathcal{T}}(L_H + \Gamma)(\lambda^k), \end{aligned}$$

where the last inequality comes from the boundedness of the gradient estimation error. Using Lemma 1 for $(a^k)_{k \in \mathbb{N}^+} = (\lambda^k)_{k \in \mathbb{N}^+}$ and $(b^k)_{k \in \mathbb{N}^+} = (\|\nabla_{\theta} \hat{H}(\theta^k)\|)_{k \in \mathbb{N}^+}$ we conclude

$$\|\nabla_{\theta} H(\theta^k)\| \xrightarrow{a.s.} 0 \quad (14)$$

I Objective functions as control problems

In this section, we show a reformulation of two common objective functions used in our experiments as Lagrangian control problems:

- **Mean-squared error:** For every data point x , the L_2 distance is used to learn a reconstruction of x with a latent dynamical state y_u “decoded” by some function g in $\mathcal{C}_{loc}^1(\mathcal{U}, X)$ (typically a neural network):

$$\begin{aligned}
 L(x, u) &= \|x - g(y_u, t_1)\|_2^2 \\
 &= \sum_{i=1}^n \left[x_i^2 - 2x_i g_i(y_u, t_1) + g_i(y_u, t_1)^2 \right] \\
 &= \sum_{i=1}^n \left[x_i^2 + 2x_i \int_{t_0}^{t_1} \partial_t (g_i(y_u, t)) dt + \int_{t_0}^{t_1} \partial_t (g_i^2(y_u, t)) dt \right] + C \\
 &= \int_{t_0}^{t_1} \sum_{i=1}^n y_u(t)^T \left[\nabla_y g_i(y_u, t) + \nabla_y g_i(y_u, t) \cdot g_i(y_u, t) \right] dt + C \\
 &= \int_{t_0}^{t_1} \sum_{i=1}^n f(y_u(t), u(t), t)^T \left[\nabla_y g_i(y_u, t) + \nabla_y g_i(y_u, t) \cdot g_i(y_u, t) \right] dt + C
 \end{aligned}$$

Given the regularity hypotheses on g , f and y , this problem takes the form (\mathcal{P}_ℓ) , and we can apply the resolution method proposed in section 4.1. **\mathcal{KL} -divergence:** Conversely, removing the decoding function g for clarity and given a target distribution $p(x)$, it is possible to define a “controlled” distribution $q_u : \int_{\Omega} y_{u(x)}(t_1) d\mathbb{P}_x$ described by the final state of the controlled dynamic $y_{u(x)} : t \mapsto X$. We can then optimize the control inference mapping to minimize the cross-entropy between the final state of the dynamic and the distribution.

$$L(p, q) = \mathcal{KL}(p(x) || q_u(x)) \quad (15)$$

$$= - \int_{\Omega} p(x) \log(y_{u(x)}(t_1)) d\mathbb{P}_x + C \quad (16)$$

$$= - \int_{\Omega} p(x) \int_{t_0}^{t_1} \partial_t (\log(y_{u(x)}(t))) dt d\mathbb{P}_x + C \quad (17)$$

$$= - \int_{\Omega} \int_{t_0}^{t_1} p(x) \frac{\dot{y}_{u(x)}(t)}{y_{u(x)}(t)} dt d\mathbb{P}_x + C \quad (18)$$

$$= - \int_{\Omega} \int_{t_0}^{t_1} p(x) \frac{f(y_{u(x)}(t), u(x), t)}{y_{u(x)}(t)} dt d\mathbb{P}_x + C \quad (19)$$

$$(20)$$

provided $y_{u(\theta, x)}(t) \neq 0$ over Ω . In practice, the estimation of the outer integral is performed with discrete empirical sampling of the data distribution.

J Experimental results

J.1 AutoencODE architectures

Adapting the models adopted by [27] and [26], we use a latent space dimension of 25 for MNIST, 128 for CIFAR-10 and 64 for CelebA. All convolutions and transposed convolutions have a filter size

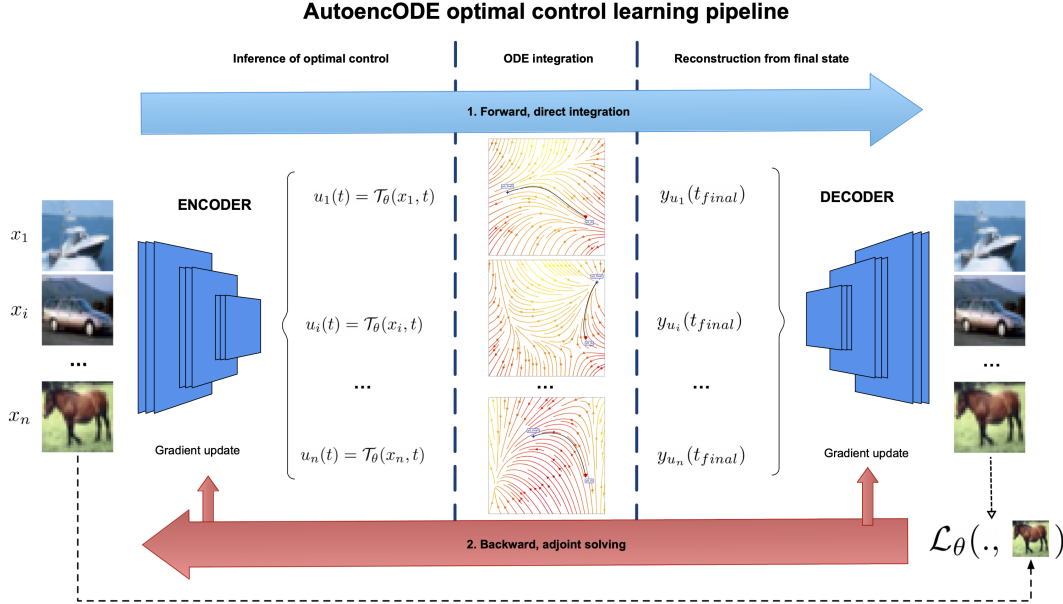


Figure S8: Diagram of our proposed model. The architecture remains very similar to a vanilla auto-encoder. The encoder is composed of a cascade of convolutional filter with non-linear activation functions followed by a linear layer that maps the activation features to the control of the latent dynamical system solved on $[t_0, t_1]$. The final state of the system is further processed by a decoding function composed of transposed convolutional filters. The model parameters are optimized for a standard objective function, with gradients estimated as a combination of backpropagation/chain-rule and the adjoint method.

	MNIST	CIFAR-10	CelebA
	$\mathbf{x} \in \mathbb{R}^{3 \times 28 \times 28}$	$\mathbf{x} \in \mathbb{R}^{3 \times 32 \times 32}$	$\mathbf{x} \in \mathbb{R}^{3 \times 64 \times 64}$
Encoder:	Flatten FC ₄₀₀ \mapsto Relu FC ₂₅ \mapsto Norm	Conv ₂₅₆ \mapsto BN \mapsto Relu Conv ₅₁₂ \mapsto BN \mapsto Relu Conv ₁₀₂₄ \mapsto BN \mapsto Relu FC _{128*2} \mapsto Norm	Conv ₂₅₆ \mapsto BN \mapsto Relu Conv ₅₁₂ \mapsto BN \mapsto Relu Conv ₁₀₂₄ \mapsto BN \mapsto Relu FC _{64*10} \mapsto Norm
Latent dynamics:	ODE[0,10]	ODE[0,10]	ODE[0,10]
Decoder:	FC ₄₀₀ \mapsto Relu FC ₇₈₄ \mapsto Sigmoid	FC _{1024*8*8} \mapsto Norm ConvT ₅₁₂ \mapsto BN \mapsto Relu ConvT ₂₅₆ \mapsto BN \mapsto Relu ConvT ₃	FC _{1024*8*8} \mapsto Norm ConvT ₅₁₂ \mapsto BN \mapsto Relu ConvT ₂₅₆ \mapsto BN \mapsto Relu ConvT ₃

Table S1: Model architectures for the different data sets tested. FC_n and Conv_n represents respectively fully connected and convolutional layer with n output/filters. We apply a component-wise normalisation of the controls components which proved crucial for good performance of the model. The dynamic is ran on the time segment [0,10] which empirically yield good results.

of 4×4 for MNIST and CIFAR-10 and 5×5 for CELEBA. They all have a stride of size 2 except for the last convolutional layer in the decoder. We use Relu non-linear activation and batch normalisation at the end of every convolution filter. Official train and test splits are used for the three datasets. For training, we use a mini-batch size of 64 in MNIST and CIFAR and 16 for CelebA in AutoencODE. (64 for control models.) All models are trained for a maximum of 50 epochs on MNIST and CIFAR and 40 epochs on CelebA.

J.2 Visualization of latent code dynamical evolution

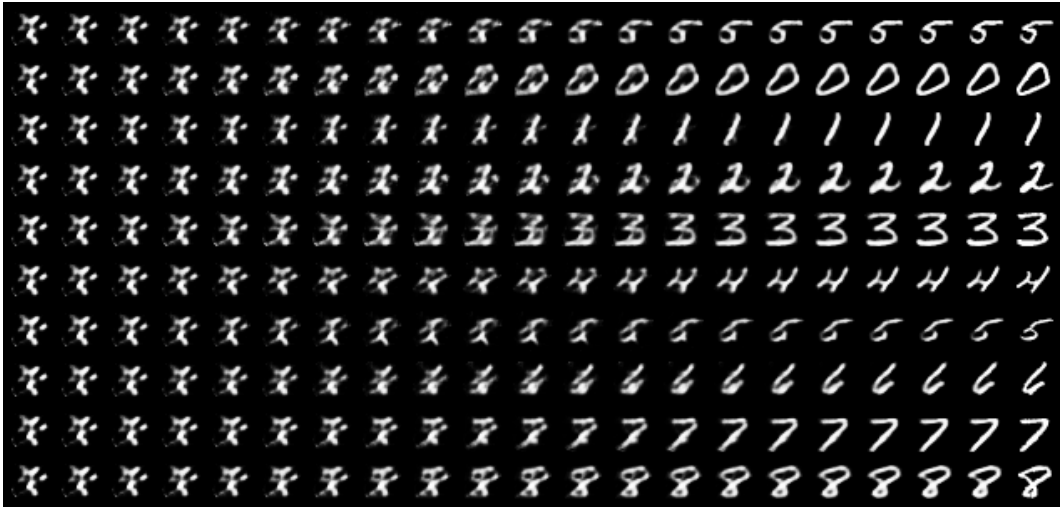


Figure S9: Reconstructions of the image along the controlled *orbits* of AutoencODE for MNIST. The temporal dimension reads from left to right. Last column: ground truth image



Figure S10: Reconstructions of the image along the controlled *orbits* of AutoencODE for CIFAR-10. The temporal dimension reads from left to right. Last column: ground truth image.



Figure S11: Reconstructions of the image along the controlled *orbits* of AutoencODE for CelebA. The temporal dimension reads from left to right. Last column: ground truth image

J.3 Exploring sampling distributions

For random samples evaluation, we train the VAE with a $\mathcal{N}(0, I)$ prior. For the deterministic models, samples are drawn from a mixture of multivariate gaussian distributions fitted using the testing set embeddings. The distribution is obtained through Expectation-Maximization [49] with one single k-means initialization, tolerance $1e^{-3}$ and run for at most 100 iterations. We compute the FID using 10k generated samples evaluated against the whole test set for all FID evaluations, using the standard 2048-dimensional final feature vector of an Inception V3 following [40] implementation.

Further experiments showed that 10K components (matching the number of data points in the test sets) logically overfits on the data distribution. Generated images display marginal changes compared to test images. However, 1000 components does not, showing that our AutoencODE sampling strategy describe a trade-off between sample quality and generalization of images. We alternatively tested non-parametric kernel density estimation with varying kernel variance to replace our initial sampling strategy. We report similar result to gaussian mixture with an overall lower FID of AutoencODE for small variance kernels. As the fitting distribution becomes very rough ($\sigma \sim 5$), the generated image quality is highly deteriorating. (see Figure S6).

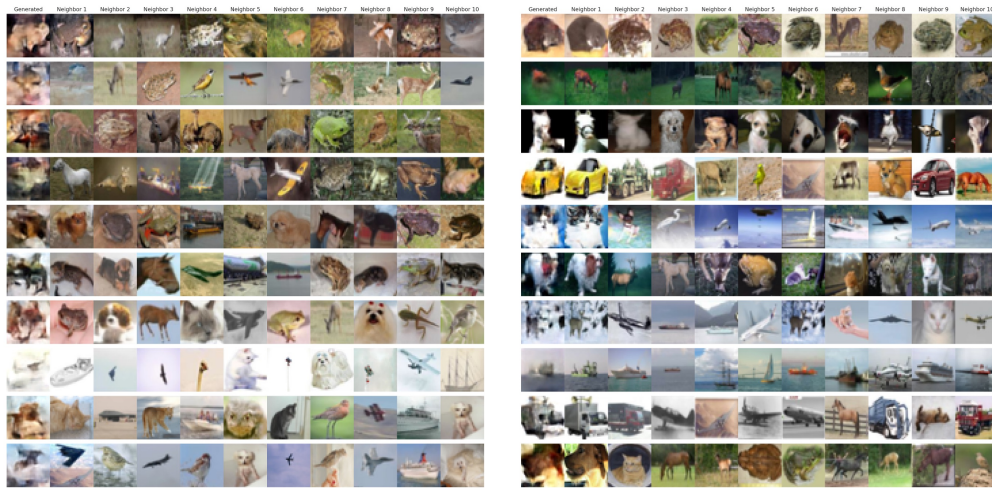


Figure S12: Nearest neighbors search of random samples from the gaussian mixture with **(Left)** 1000 components **(Left)** and **(Right)** 10K components in the testing set of CIFAR-10.

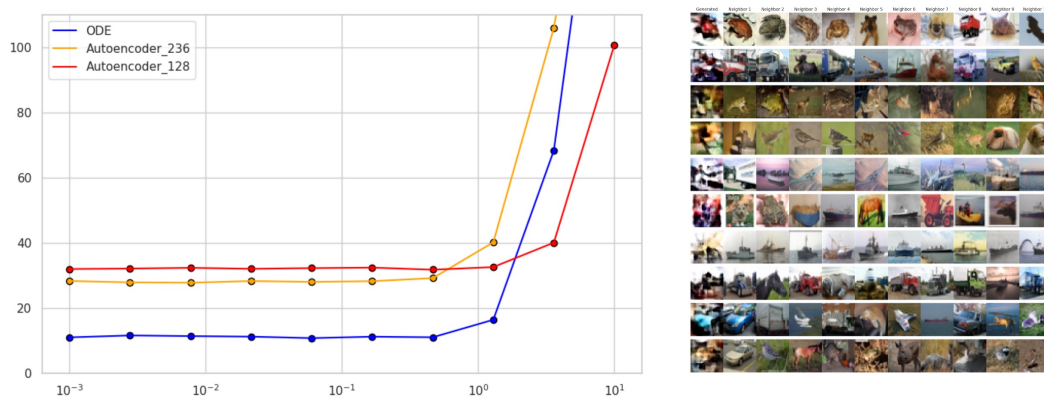


Figure S13: **(Left)** Evolution of FID between test set and generated samples as a function of the gaussian kernel variance used to perform kernel estimation of the the latent code distribution. **(Right)** Nearest neighbors search of random samples from the latent distribution fitted with a gaussian kernel estimation with variance $\sigma = 2$ in the testing set.

J.4 Latent code interpolation



Figure S14: Interpolation experiments: We further explore the latent space of AutoencODE by interpolating between the latent vectors of the **CelebA** test set. (**Upper panel**) Linear interpolation between random samples reconstructed with AutoencODE. (**Middle panel**) Interpolation comparison between AutoencODE and a vanilla auto-encoder for a single pair of vectors. (**Lower panel**) 2d interpolation with three anchor reconstructions corresponding to the three corners of the square (A:up-left,B:up-right and C:down-left. Left square corresponds to AutoencODE reconstructions and right to a vanilla auto-encoder.

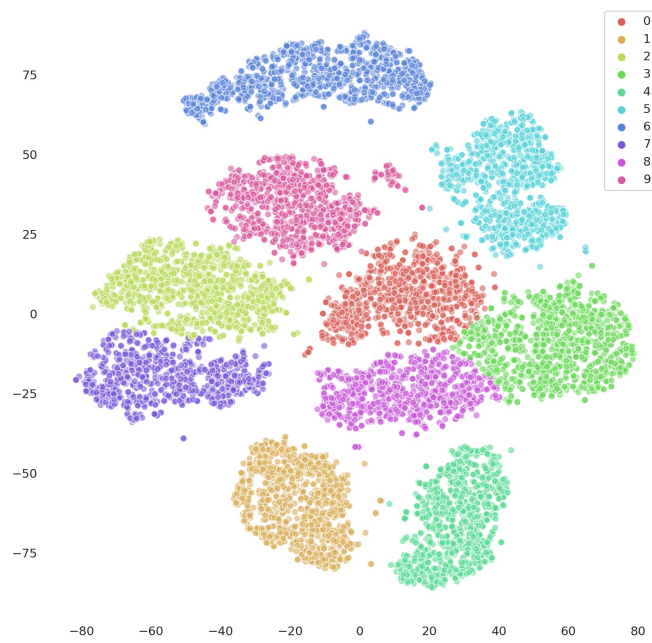


Figure S15: tSNE embeddings of the latent code at $t = t_1$ for MNIST test set colored with a 10 component gaussian mixture model.